We are IntechOpen, the world's leading publisher of Open Access books Built by scientists, for scientists

4,800
Open access books available

122,000
International authors and editors

135M
Downloads

Our authors are among the

154
Countries delivered to

TOP 1%
most cited scientists

12.2%
Contributors from top 500 universities

CLARIVATE ANALYTICS BOOK CITATION INDEX INDEXED

WEB OF SCIENCE™

Selection of our books indexed in the Book Citation Index in Web of Science™ Core Collection (BKCI)

Interested in publishing with us?
Contact book.department@intechopen.com

Numbers displayed above are based on latest data collected.
For more information visit www.intechopen.com

Chapter 6

Catalytic Steam Reforming of Methanol to Produce Hydrogen on Supported Metal Catalysts

Raúl Pérez-Hernández, Demetrio Mendoza-Anaya,
Albina Gutiérrez Martínez and Antonio Gómez-Cortés

Additional information is available at the end of the chapter

http://dx.doi.org/10.5772/49965

1. Introduction

The use of fossil fuels for energy supply in the world has caused various global environmental problems. For this reason it is becoming progressively more important to find ways of providing environmentally friendly energy. One promising alternative to fossil fuels is hydrogen, due to the importance as a clean source of energy, as well as, the increased demand in chemical industry [1; 2]. Also, fuel cells have recently attracted much attention as a potential device for energy transformation. Their performance is based on a clean process, without forming harmful by-products such as sulphur oxides and nitrogen oxides, while having a highly efficient energy transformation compared to conventional power generation processes as in heat engines. Hydrogen is a promising fuel for fuel cells and can be produced by steam reforming of natural gas, methanol and gasoline. At present, most of the world's hydrogen is produced from natural gas (~97 % CH_4) by a process called steam reforming [3-8]. The primary ways in which methane, is converted to hydrogen involve reaction with either steam (steam reforming), oxygen (partial oxidation), or both in sequence (autothermal reforming). In practice, gas mixtures containing carbon monoxide, carbon dioxide and unconverted methane. Reaction of carbon monoxide with steam (water-gas shift) over a catalyst produces additional hydrogen and carbon dioxide, and after purification, high-purity hydrogen is recovered. This reaction is highly endothermic. Although stoichiometry for the SRM suggests that only one mole of water is required for one mole of methane ($CH_4 + H_2O \rightarrow CO + 3H_2$), usually excess steam is used to reduce carbon formation. In most cases, carbon dioxide is vented into the atmosphere today, but there are options for capturing it in centralized plants for subsequent sequestration. However, steam reforming of methane does not reduce the use of fossil fuels and it still releases carbon to the environment in the form of CO_2. Thus, to achieve the benefits of the hydrogen economy, it is necessary produce hydrogen from non−fossil resources, such as water, methanol or ethanol

using a renewable energy source. Among the different feedstocks available, alcohols are very promising candidates because these are easily decomposed in the presence of water and generate hydrogen-rich mixture at a relatively lower temperature. Steam reforming (SR) of methanol has been extensively studied in recent years [1–7]. Methanol has a low boiling point, a high hydrogen/carbon ratio and no C–C bonds, and can therefore be reformed at a relatively low temperature, reducing the risk of coke formation during the reaction [9]. Moreover, as methanol can be produced from renewable sources, its reforming does not contribute to a net addition of CO_2 to the atmosphere. Methanol can be converted to hydrogen by the following three reactions:

Partial oxidation of methanol

$$CH_3OH + 0.5O_2 = 2H_2 + CO_2 \qquad \Delta H^\circ = -192\ \text{kJ mol}^{-1} \tag{1}$$

Steam reforming of methanol

$$CH_3OH + H_2O = 3H_2 + CO_2 \qquad \Delta H^\circ = 50\ \text{kJ mol}^{-1} \tag{2}$$

Oxidative Steam Reforming of Methanol

$$CH_3OH + 1/2H_2O + 1/4O_2 = CO_2 + 5/2H_2 \qquad \Delta H^\circ = 0\ \text{kJ mol}^{-1} \tag{3}$$

Most studies reported in the literature for the steam reforming reaction were on the application of CuO/ZnO-based and CuO/ZnO/Al_2O_3-based catalysts [10-12]. Alumina is generally added to the catalysts to improve their surface area and mechanical strength, and to prevent catalyst sintering [13]. The in situ characterization of CuO/ZnO reveals that the interaction of Cu and ZnO has a pronounced effect on the catalytic activity [14; 15]. Zinc oxide is known to improve the dispersion of Cu and the reducibility of CuO. The improvement of reducibility has been proposed as a possible cause of the good activity of CuO/ZnO-based catalysts [16]. However, some researchers have proposed that the main reason is the improvement in the adsorption properties, including the adsorption of methanol [17] and the spillover of both hydrogen from Cu to ZnO [18] and oxygen species from ZnO to Cu [19]. ZrO_2 addition to Cu-based alumina-supported catalysts has been shown to increase methanol conversion and reduce CO yields [9; 20]. However, it has been noted that the metal–support interactions in Cu/ZrO_2 are different than in the more conventional Cu/ZnO catalysts [21]. Some authors even describe a ''synergy'' between the Cu and ZrO_2 [13]. The higher activity of Cu-ZrO_2 catalysts has also been attributed to the stabilization of Cu_2O on the surface of the reduced catalysts or during the reaction [22; 23]. It is believed that the formation of Cu_2O leads to both more active and more durable catalysts, since Cu_2O is less susceptible to sintering compared with Cu metal [22; 23]. Cu^+ species have also been observed in CeO_2-containing Cu catalysts [24; 25] and isolated Cu^{2+} in lattice sites or in surface sites forming a nano-sized two-dimensional structure [26]. Addition of CeO_2 to Cu/Al_2O_3 catalysts has also been shown to increase methanol conversion, decrease CO selectivity and increase catalyst stability [27]. Due to this a strong effort has been directed to

increase the overall efficiency of CeO_2 for different applications. CeO_2 has been widely used in purifying vehicle exhausts and became the most important rare oxides for NOx reduction with CO or hydrocarbons [28; 29]. Numerous studies of ZrO_2 or CeO_2 promoted Cu-based methanol steam reforming catalysts are available in the literature [10; 12; 21; 25; 27; 30-34]. However, comparing results between studies is challenging since the reaction evidently is very sensitive to the catalysts used and large differences in Cu loadings and catalyst compositions have been reported. For example, the copper concentrations on these types of catalysts have been varied from a few percent in some publications [35; 36] up to 70% or above in others [13]. Other studies related with nickel based catalysts on the methanol reforming process has been reported [37-39] or ethanol (SRE) as an H_2 source [40-44]. Navarro et al. [45] studied the oxidative reforming of hexadecane over Ni and Pt catalysts supported on Ce/La-doped Al_2O_3. They found for both Ni and Pt catalysts, higher specific activity when active metals were supported on alumina modified with cerium and lanthanum. However, the catalytic activity and H_2 selectivity observed on Ni-based catalysts were higher than on Pt-based catalysts. Recently, Pd-ZnO catalyst systems have been reported to be active and selective for MSR after pre-reducing with H_2 [46-48] and Pd supported on ZrO_2-TiO_2 [49]. Other catalytic systems containing highly dispersed gold have received great interest from both experimental and theoretical points of view. The role of metal oxide is to stabilize the gold nanoparticles and make the reaction take place on the gold surface reaction. Due to their high catalytic activity, particularly in CO oxidation at low temperature [50] gold-base catalysts are considered promising candidates for hydrogen production, through methanol decomposition and water-gas shift (WGS) reactions [51-54] catalytic combustion of volatile organic compounds (VOCs) [55], selective oxidation of CO in H_2-rich gas [56], adsorption of CO on Au/CeO_2 catalysts [57]. Methanol steam reforming for H_2 production has been not studied extensively with Au-base catalysts. Nevertheless, some gold-base catalysts has shown high activity for methanol oxidation at 373 K but low H_2 production as a function of time on stream [58]. On methanol decomposition was reported that gold supported on Al_2O_3 was most active than on the CeO_2, however, on the last catalyst the H_2 selectivity was better than on the former catalyst on the range temperature of 300 to 500 °C [58]. But, when water was added in the feed they observed a slight increase in the methanol conversion and, changes in the products distribution. The catalytic activity of the Au-Ag/CeO_2 catalyst and silver supported on ZnO 1D rods catalysts on the steam reforming methanol reaction for hydrogen production was reported [59-61]. The catalytic activity on Ag/ZnO sample with low Ag content showed better performance on the SRM reaction than on high silver loading catalyst. So, the sample with small Ag particle size showed best performance in methanol conversion than catalyst with big Ag particle size. Our group has previously studied the effect of nickel-copper addition to ZrO_2 by impregnation method and compared the catalytic activity of these bimetallic Cu/Ni catalysts on the oxidative steam reforming of methanol to produce H_2 [39]. The reactivity of the catalysts showed that the bimetallic samples prepared by successive impregnation had highest catalytic activity among all the catalysts studied.

The goal of this chapter is showed the effect of the metal copper or nickel addition to CeO_2 prepared by co-impregnation and sequential impregnation. Catalytic performance in oxidative steam reforming of methanol for the three Cu–Ni catalysts was compared with corresponding monometallic Cu and Ni catalysts, and Au/CeO_2 catalysts. The comparison is also made with characterization results obtained by BET (N_2 adsorption–desorption), SEM (Scanning Electron Microscopy), EDX (Energy Dispersive X-ray Spectroscopy), XRD (X-ray Diffraction), TEM (Transmission Electron Microscopy) and TPR (Temperature Programmed Reduction). In addition, the relation between the structure of bimetallic particles and catalytic performance in oxidative steam reforming of methanol is discussed.

2. Experimental

2.1. Synthesis of the catalysts

The CeO_2 synthesis was done using the precipitation method of the $Ce(NO_3)_3 \bullet 6H_2O$ (Aldrich) in NH_4OH (Fluka) at room temperature (r.t.).

$$8Ce(NO_3)_3 \bullet 6H_2O + 22NH_4OH \leftrightarrow 8Ce(OH)_4 \downarrow + 23NH_4NO_3 + 41H_2O \quad (4)$$

$$Ce(OH)_4 \xrightarrow{\Delta} CeO_2 + 2H_2O \quad (5)$$

The solid obtained was dried at 100 °C and then heated at 650°C for 5 hours in air stream. The prepared supports were impregnated with a solution of $NiCl_2 \bullet 6H_2O$, and another with a solution of $Cu(CH_3\text{-}CO_2)_2 \bullet H_2O$ at an appropriate concentration to yield 3 wt% of copper and nickel respectively. Three bimetallic samples were prepared at 50%Cu and 50%Ni respectively to obtain 3 wt. % of total metallic phase. For the first sample, CeO_2 support was successively impregnated with an aqueous solution of $Cu(CH_3COO)_2 \bullet H_2O$ (Merck), after that, the excess of water was removed at 80 °C under constant stirring and the catalyst was dried at 110 ºC and calcined at 500 °C for 2 h followed by cooling down to r.t. Then, an aqueous solution of $NiCl_2 \bullet 6H_2O$ was added and the resulting solid was calcined at the same temperature and time. The as prepared catalysts will be referred as Ni/Cu/CeO_2. For the second catalyst, the synthesis procedure was changed to the above sample mentioned. The labeling of this catalyst will be referred as Cu/Ni/CeO_2. The third sample (Cu-Ni/CeO_2) was prepared by using a simultaneous impregnation (also called co-impregnation): an aqueous solution of $Cu(CH_3COO)_2$ and $NiCl_2 \bullet 6H_2O$ were added to CeO_2 and calcined at 500 °C for 2 h. All the samples were reduced at 400 °C using a mixture of H_2 (5%)/He (50 mL/min) stream for 1 h before characterization, except for TPR technique in which the sample was calcined.

2.2. Characterization

The details of catalysts characterization have been reported in our earlier reports [26; 28; 37; 38; 49; 59; 61-64]. Nitrogen adsorption-desorption of the samples was measured at -196 C on a Belsorp-max Bel Japan equipment. Prior to the measurements the samples were degassed at 150 °C for 1 h. The surface area and pore size distribution were determined using the BET

and BJH methods respectively. HRTEM and local chemical analysis of the bimetallic nanoparticles were carried out in a JEM 2200FS microscope with a resolution of 0.19 nm and fitted with an energy dispersive X-ray Spectrometer (NORAN) and a JEM 2010-HT with a point resolution of 0.19 nm fitted with an EDX microprobe Thermo-scientific. JEOL-2010 microscope with a point resolution of 0.19 nm fitted with an NORAN microprobe Thermo-scientific. The samples were dispersed in isopropanol and a drop of such a solution was placed onto copper and gold 300 mesh grids. Surface properties of the catalysts were studied by CO adsorption followed by DRIFT (Fourier Transform Infrared Spectroscopy). Experiments were done in a Nicolect Nexus 470 Spectrometer equipped with environmentally controlled Spectra Tech DRIFT (Diffuse Reflectance Infrared Fourier Transform) cell with KBr windows. For each experiment, 0.025 g of the sample was packed in the sample holder and pretreated in-situ under H_2 flow (30 mL/min) at 300 °C for 1 h. After this treatment the sample was purged with helium flow for half hour and cooled to room temperature in the same gas atmosphere before admittance for 5 min a flow (30 mL/min) of 2.5 %CO diluted in He. Afterwards, pure He was allowed to flow in the system to eliminate the residual CO gas. Spectra were collected from 128 scans with resolution of 4 cm^{-1}. For all catalysts a FTIR spectrum was obtained by making reference to the freshly reduced solid prior to CO adsorption. The spectrum of dry KBR was taken for IR single-beam background subtraction. Oxidative steam reforming of methanol was carried out at an atmospheric pressure by placing the fixed bed flow reactor (8 mm i.d.) in an electric furnace consisting of two heating zones equipped with omega temperature controllers, using a commercial flow system RIG-100-ISRI. Prior to OSRM reaction, 0.05 g of catalyst diluted in 0.150 g of SiC was reduced in situ, using a stream of H_2 (50 mL/min) increasing temperature from room to 400 °C with a heating rate of 10 °C/min and holding this temperature for 1h. A thermocouple in contact with the catalytic bed was utilized in order to monitor and control the temperature inside the catalyst. For the reaction, O_2 (5%)/He mixture (50 mL/min) and 150 mL/min of He was passed through stainless steel saturator containing methanol and water mixture (we use a hot line in the saturator in order to maintain constant the temperature ~ 25 °C). This gas was added by means of a mass flow controller (RIG-100). The total flow rate was kept at 200 mL/min. Reaction products were analyzed by Gow-Mac 580 Gas chromatograph with thermal conductivity detector equipped with two columns system (molecular sieve 5 Å and Porapack Q columns), double injector controlled by Clarity software V.2.6.04.402 and TCD. The first column was used to separate the gaseous products such as H_2, O_2, CH_4 and CO. The second column was used to separate water, methanol, methyl formate (MF) and CO_2. All the reported data were collected after a run time of 7 h. The following equations were used to determine the methanol conversion and selectivity:

$$X(\%) = \frac{C_{in} - C_{out}}{C_{in}} * 100 \quad S_{CO_2}(\%) = \frac{nCO_{2-out}}{nCO_{2-out} + nCO_{out}} * 100$$

and/or

$$S_{H_2}(\%) = \frac{nH_{2-out}}{nH_{2-out} + nCH_{4-out} + nCO_{2out} + CO} * 100$$

The subscripts in and out indicate the inlet and the outlet concentrations of the reactants or products.

3. Results

3.1. Ni/Cu/CeO_2 system

3.1.1. Textural properties of the Cu-Ni/CeO_2 system

Table 1 showed the textural properties of the catalytic materials obtained from N_2 physisorption measurement at temperature of liquid nitrogen. It showed that doping the bare CeO_2 support with copper or nickel to obtain the monometallic catalysts, results in a slight decrease on the BET surface area. The same effect was observed on the bimetallic samples, when Cu and Ni were impregnated by successive or co-impregnation method on the CeO_2. Typical SEM image with backscatter analysis of the as-synthesized Cu-Ni/CeO_2 catalyst prepared by co-impregnation method is present in Fig. 1. It showed that the sample is composed by irregular particles. It is important to mention that the bare CeO_2, as well as, the other catalysts under study had the same morphology, as the sample present on Fig. 1. This is expected because we used the CeO_2 previously stabilized at 650 °C to obtain the catalysts.

Sample	m^2/g
CeO_2	40.1
Cu/CeO_2	34.5
Cu/Ni/CeO_2	25.7
Cu-Ni/CeO_2	30.4
Ni/Cu/CeO_2	27.5
Ni/CeO_2	28.6

Table 1. Specific surface area (BET) of the Ni/Cu-base catalysts.

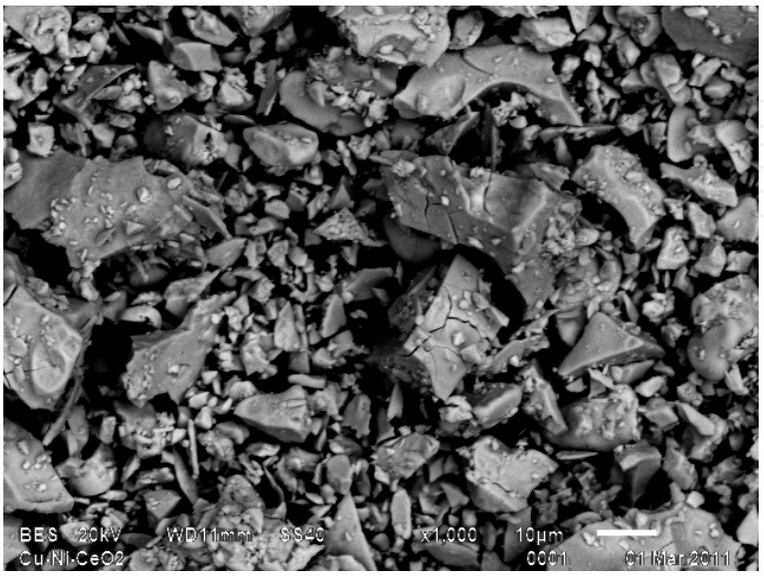

Figure 1. Typical SEM image of the fresh Ni-Cu/CeO_2 prepared by co-impregnation.

3.1.2. Crystalline phases of the Cu-Ni/CeO2 catalysts

Fig. 2 showed the XRD patterns of the Ni/Cu/CeO_2 catalysts after thermal treatments (calcination and reduction). XRD patterns of the Ni/Cu-base catalysts yield a typical cubic fluorite structure of ceria, in addition, diffraction peak attributed to the metallic Ni was observed at 2Θ= 44.735 on the Ni/CeO_2 sample, indicating that NiO was completely reduced to metallic Ni below 500 °C. On Cu/CeO_2 sample diffraction-peaks of metallic Cu were observed at 2Θ = 43.317 and 50.449 (JCPDS 85-1326) respectively. On the bimetallic samples, diffraction peaks of Cu, Ni or Cu-Ni alloy were not observed, although the samples suffer different thermal treatments; this could be due to its low metal concentration (3.0 wt %) or because the particle size of the active phase is below of the detection limit of the technique. On samples with 3 wt. % of Cu/Ni supported on ZrO_2 [39] was observed the same effect. So, no diffraction peaks of metallic phase were observed by XRD technique.

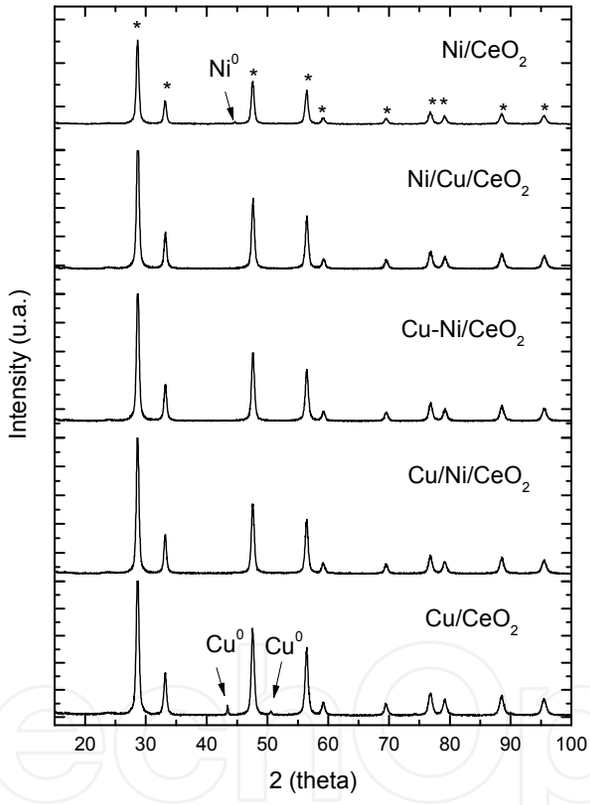

Figure 2. XRD patterns of the Ni/Cu/CeO2 catalysts. [*] cubic -CeO2

3.1.3. Temperature-programmed reduction of the Cu-Ni-base catalysts supported on CeO2

Hydrogen consumption curves of the fresh bimetallic Cu/Ni-base catalysts and samples after catalytic reaction are shown in Fig. 3. Although the position of the reduction peaks strongly depends of the particle size or the interaction between metal active phase and the support, the TPR profiles of the catalytic materials are included for comparison. TPR profile of the bare CeO_2 sample showed a broad peak above 500 °C, this is assigned to reduction of surface ceria. Calcined CuO/CeO_2 catalyst showed three reduction peaks below 300 °C

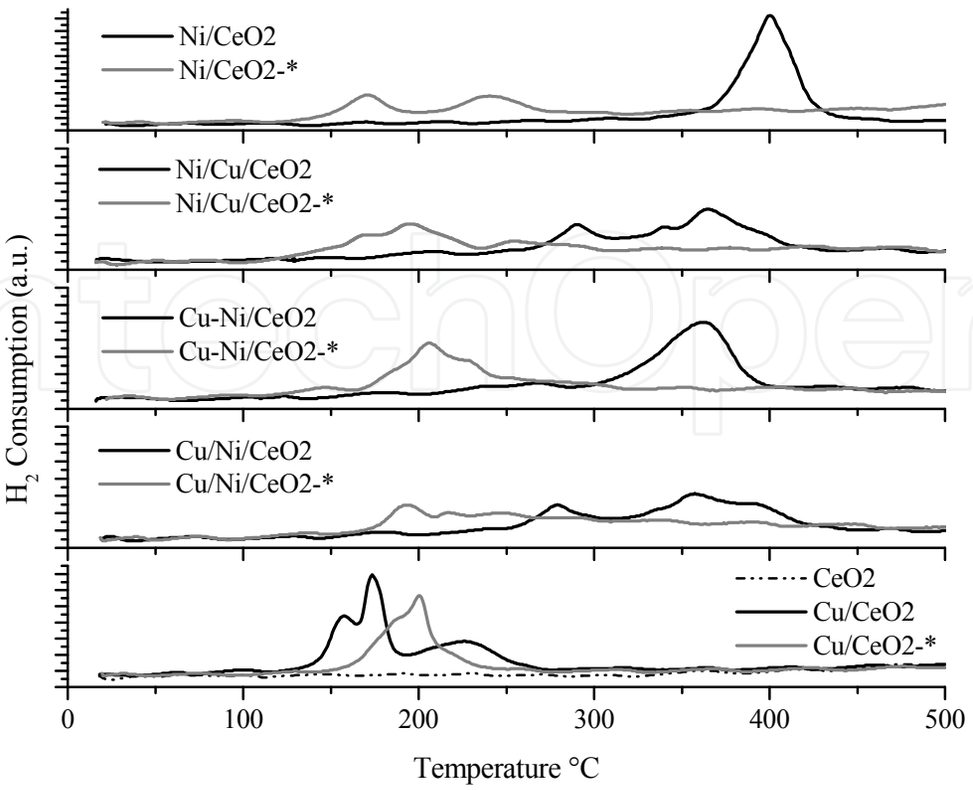

Figure 3. Temperature-programmed reduction profiles of the fresh Cu/Ni/CeO_2 catalysts (solid line) and samples after catalytic reaction (clear line).

indicating the presence of different kinds of Cu species formed during the preoxidation step [26; 63]. Peaks below 200 °C were attributed to reduction of highly dispersed CuO and the peak above 200 °C was associated with the reduction of the CuO bulk. The NiO/CeO_2 catalyst showed a sharp reduction peak at around 400 °C and may be attributed to reduction of NiO to metallic Ni crystallites. This temperature is higher than that the reported in previous work [38] for a similar catalyst. In that case the Nickel precursor was $Ni(NO_3)_2 \bullet 6H_2O$ which indicates different interaction between NiO and CeO_2. TPR profile of the bimetallic catalysts showed reduction peaks at lower temperature than Ni/CeO_2 catalyst. It has been reported that NiO supported, could be reduced at low temperatures when Cu or Pt are presented [37; 39; 65]. Because, Cu or Pt causes spillover of hydrogen onto Ni, inducing a simultaneous reduction of both, copper (platinum) oxide and NiO, causing a shift in the reduction of the active phase at low temperatures. In addition, it has been suggested that the first reduction peak observed in the TPR profile of the bimetallic catalyst, corresponded to the reduction of adjacent Cu and Ni atoms, which could be forming a bimetallic phase [37; 39; 65]. This finding indicates that the bimetallic phase had different interaction with the support and promoted the nickel reduction at lower temperatures and slows the copper reduction. In addition, it is clear that the bimetallic samples prepared by successive impregnation showed a broader reduction peak at higher temperatures than that for the Cu/CeO_2 sample, suggesting a broad particle size distribution, and slightly lower than Ni/CeO_2 sample. On the other hand, the TPR profiles of the Ni/CeO_2 and Ni-Cu/CeO_2

samples showed a sharp reduction peak than the rest of the samples. The sharp peak observed on theses samples corresponds to high uniformity in the Ni crystallite size. TPR profiles of the samples after catalytic reaction showed lower H_2 consumption, indicating that under OSRM conditions the active phase is partial oxidized. On Cu/CeO_2 samples was found by EPR technique the presence of the ion Cu^{2+} forming a nano-sized two-dimensional structure after OSRM reaction [26; 66; 67]. Oguchi et al. [22] observed a reduction peak on the CuO/ZrO_2 sample post-reaction. They concluded that the Cu_2O catalyst was stabilized during the SRM reaction. Turco et al. [68] suggested that there was a zone within the catalytic bed where the catalyst is oxidized, and another zone where it was reduced. This phenomena could be occurred on our samples, because, generally in oxidative steam reforming process, evidence suggest that the front of the catalyst bed is partially oxidized and the downstream of the catalyst bed remains in the reduced state.

3.1.4. DRIFTS of CO adsorption

In situ DRIFT spectra of the monometallic Ni/CeO_2 and Cu/CeO_2 samples and the three bimetallic Cu/Ni-base samples exposed to a 2.5%CO/He gas mixture recorded at room temperature with the aim to evaluate the influence of the metal addition to CeO_2 on the type and amount of different surface species. Fig. 4 shows an infrared spectrum in the 2200–2000 cm^{-1} regions of the Cu/Ni-base catalysts. The CO absorption band was observed at 2130 and 2100 cm^{-1} on the Ni/CeO_2 and Cu/CeO_2 samples respectively. It is generally acknowledged that carbonyl bands at wavenumbers lower than ca. 2115 cm^{-1} are due to carbonyl species adsorbed on metallic copper particles *[69]* while those at higher wavenumber correspond to carbonyls adsorbed on oxidized copper sites, so, the wavenumber increasing with the copper oxidation state. Variations in the frequency of these carbonyls have been related to changes in the nature of the exposed faces (i.e., in the degree of coordination of the copper centers). The main component at 2100 cm^{-1} was associated to CO adsorption on Cu sites of stepped particles (i.e., ‹110› plane) [70]. The band at 2135 cm^{-1} observed on the bimetallic samples was close to Ni/CeO2 catalyst, although it is slightly shifted to higher wavenumbers but it is virtually the same independently of the Cu and Ni addition to CO_2. In these bimetallic samples the absorption band corresponding to CO adsorption on Cu is totally suppressed (Fig. 4b). This finding suggests that the bimetallic samples are richer with Ni atoms in the surface of the catalysts. On the other hand, the high intensity in the CO-band observed on the bimetallic samples than monometallic catalysts could be associated to major dispersion of the metal active phase on the CeO_2. Differences in the CO-chemisorption were observed on the region of 1800–1000 cm^{-1} (Fig. 4c). CO chemisorption on the reduced surface CeO_2 and Mo/CeO_2 samples showed bidentate carbonate (as-1340, s-1680 and as-1320, s-1690 cm^{-1}), bicarbonate (1220, s-1460, s-1490 and as-1630 cm^{-1}), and bridged carbonate (as-1285 and s-1750 cm^{-1}) [71; 72]. No bands for the carbonate-like species was detected in the region of 1800–1000 cm^{-1} on the bimetallic samples prepared by successive impregnation as well for Cu/CeO_2 sample which indicates that CO does not adsorb on these materials.

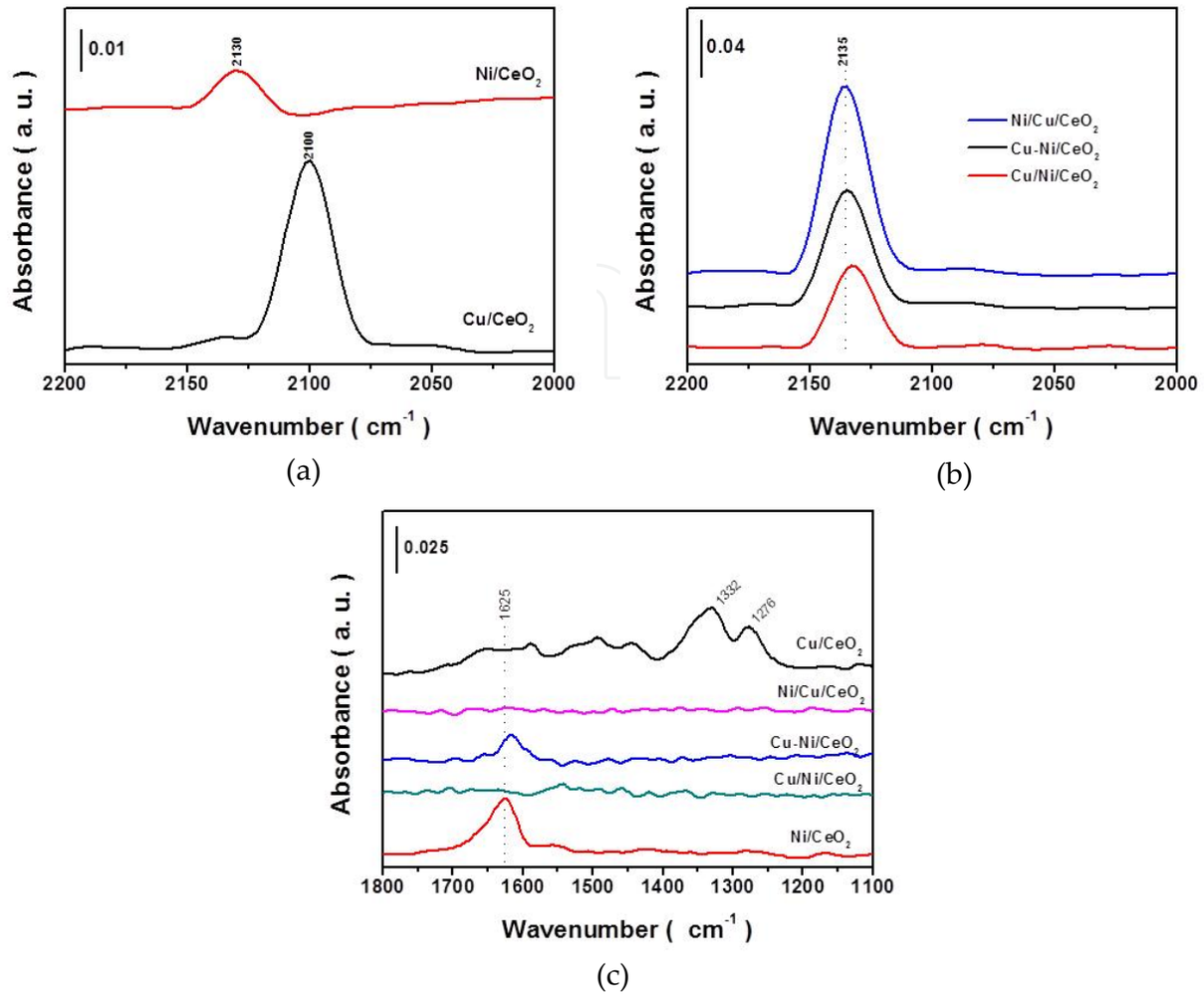

Figure 4. Diffuse reflectance FTIR spectra of CO adsorbed on monometallic-a and bimetallic-b catalysts. CO-absorption region of 1800–1000 cm^{-1} on all samples-c.

3.1.5. Catalytic activity of the Cu-Ni/CeO_2 catalysts on the OSRM reaction

The effect of the Cu and Ni addition to CeO_2 was evaluated on the oxidative steam reforming of methanol (OSRM) reaction from 200 to 400 °C. Fig. 5a-b summarizes the results of the CH_3OH conversion and H_2 selectivity over various catalysts as a function of the reaction temperature. It is clear that the bare-CeO_2 showed poor catalytic activity at the maximum reaction temperature. In general in all the samples the methanol conversion increased with an increase in the reaction temperature but, it is different when Cu and/or Ni were impregnated to CeO_2. At the beginning of the reaction the Cu/CeO_2 catalyst showed better methanol conversion than the other samples. When the temperature was raising at 300 °C the Cu/CeO_2 and the bimetallic Cu-Ni/CeO_2 (prepared by co-impregnation) catalysts had the same methanol conversion (40 %). Following by the bimetallic samples prepared by successive impregnation and the worst catalyst for methanol conversion was the Ni/CeO_2 sample. At the maximum reaction temperature the methanol conversion showed the following order: Ni/CeO_2 > Cu-Ni/CeO_2 > Ni/Cu/CeO_2 > Cu/Ni/CeO_2 > CeO_2. In previous

study was observed that when Ni was supported on CeO_2 it showed better methanol conversion than Ni/ZrO_2 sample [38]. López et al. [39] reported that the Ni/Cu/ZrO_2 and Cu/Ni/ZrO_2 catalysts prepared by successive impregnation, showed high catalytic activity and H_2 selectivity than bimetallic sample prepared by simultaneous impregnation and the monometallic catalysts on the OSRM reaction. They calculated the reactivity of the model catalysts prepared by successive impregnation and observed that the band gap of the bimetallic models decreases, then, an electron transfer mechanism is favored at the interface between the bimetallic structures and the support, facilitating the redox properties of the catalysts, giving a higher OSRM activity [39]. In our case, we observed that the Ni/CeO_2 and Cu-Ni/CeO_2 (prepared by co-impregnation) samples had the best catalytic activity at the maximum reaction temperature. On these samples was observed by DRIFT technique the CO-band at 1625 cm^{-1} which was not present on the other samples. This finding can be attributed that the CO adsorption, in the carbonate species range were not favored on the other catalysts, indicating that CO does not adsorb on these materials, and so there are some blockade sites for catalytic reaction. The selectivity towards H_2 carried out at 200–400 °C on Cu-Ni-base catalysts supported on CeO_2 catalysts increased progressively by increasing the reaction temperature. It is clear that the Ni/CeO_2 and Cu-Ni/CeO_2 catalysts showed higher selectivity toward H_2 than the others samples.

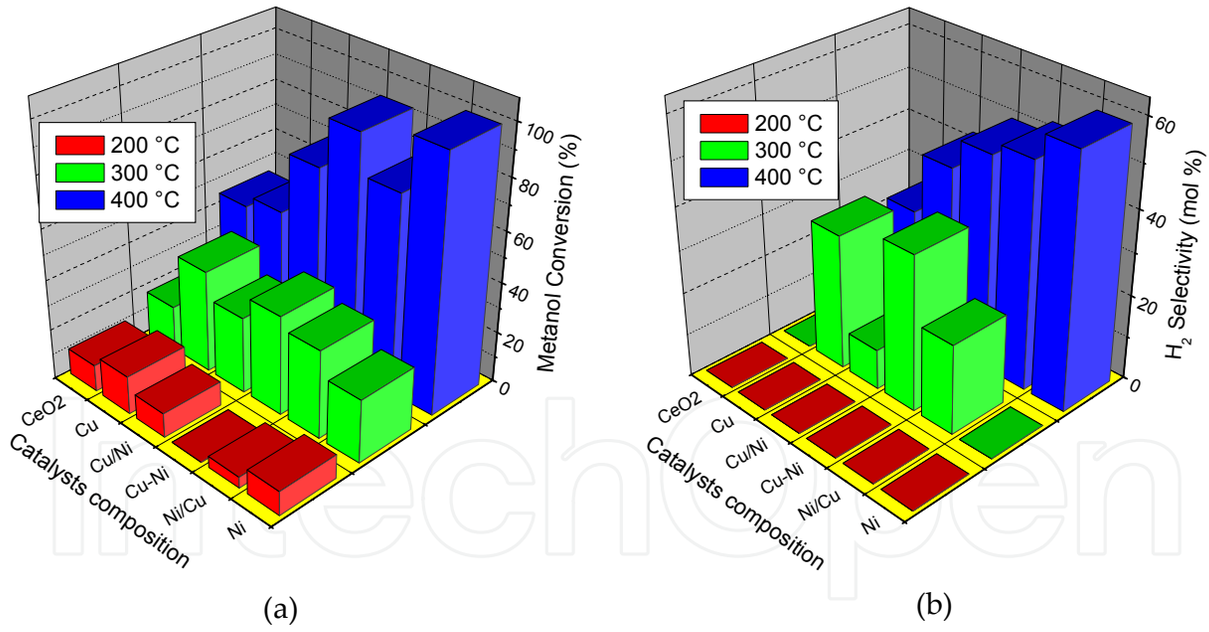

Figure 5. Methanol conversion of the Ni/Cu supported on CeO_2-(a) and H_2 selectivity-(b)

3.2. Au/CeO_2 system

3.2.1. Experimental section

CeO_2 catalyst was prepared in advance by precipitation method. NH_4OH (Baker) was added drop wise to an aqueous solution of ($Ce(NO_3)_3 \bullet 6H_2O$). The precipitated solid was

aged for 24 h and the residual liquid was removed by decanting, then the solid was dried at 100 °C for 24 h. The solid material was calcined at 100 °C 1h under an air stream and then at 500 °C for 5 h. The prepared support was impregnated with an aqueous solution of $HAuCl_4$ at an appropriate concentration to yield 1 and 3 wt % of total Au in the catalysts. The samples were dried at 100°C for 1h and then calcined at 400 °C for 2h in static air and finally reduced with a H_2(5%)/He stream at 350 °C 1h before the characterization and activity test. The labeling of different catalysts will be referred as follows: nAu/CeO_2 where n = 1 and 3 wt. % of Au in the catalyst respectively. The steady-state activity in the SRM reaction was performed in a conventional fixed-bed flow reactor (8 mm i.d.) using 0.1 g of the catalyst in a temperature range from 300 to 475 °C with steps of 25 °C with 6 h of stabilization time at each temperature and atmospheric pressure on an automatic multitask unit RIG-100 from ISR INC. The catalyst was first activated in a stream of H_2 (60 mL/min) from room temperature to 350 °C with a heating rate of 10°C/min and held at this temperature for 1h. A thermocouple in contact with the catalytic bed allowed the control of the temperature inside the catalyst was used. The sample was brought up to the reaction temperature in He and the reaction mixture was introduced. For the SRM reaction, He (60 mL/min, GHSV= 30,000 h^{-1} based on the total flow) was added by means of a mass flow controller (RIG-100) and bubbled through a tank containing mixture of water and methanol, the partial pressure of CH_3OH and H_2O was 9999.18 and 1699.86 Pa respectively. The molar ratio in the steam was CH_3OH (1.95μmol)/H_2O (1.97 μmol) = R ≈ 1.0 and the other concentration tested was CH_3OH (4.7 μmol)/H_2O (1.97 μmol) = R ≈ 2.4. The effluent gas of the reactor was analyzed by gas-chromatography (Gow-Mac 580 instrument) equipped with a two columns system (molecular sieve 5 Å and Porapack Q columns), double injector controlled by Clarity software V.2.6.04.402 and TCD. The first column was used to separate the gaseous products such as H_2, O_2, CH_4 and CO. The second column was used to separate water, methanol, methyl formate (MF) and CO_2. The GC analysis was performed in isothermal conditions (oven temperature = 100 ◦C). The equations used to determine the methanol conversion and selectivity was showed above.

4. Results and discussion

BET surface area calculated by the N_2 adsorption-desorption through the single point method of the 1Au/CeO_2 and 3Au/CeO_2 catalysts after thermal pretreatments were 44 and 34 m^2/g respectively. Figure 6 (a, b) showed a representative area of the 1Au/CeO_2 and 3Au/CeO_2 catalysts respectively. It showed that both samples are constituted by white spots identified as Au on large CeO_2 particles. Among these catalysts the sample with high Au loading showed big Au nanoparticles (large white spots) than on the 1Au/CeO_2 catalyst. Inset image in Figure 6a, showed an amplification of CeO_2 support using FE-SEM technique. Under this analysis we found that the CeO_2 is constituted by nanoparticles with diameters ~ 20 nm.

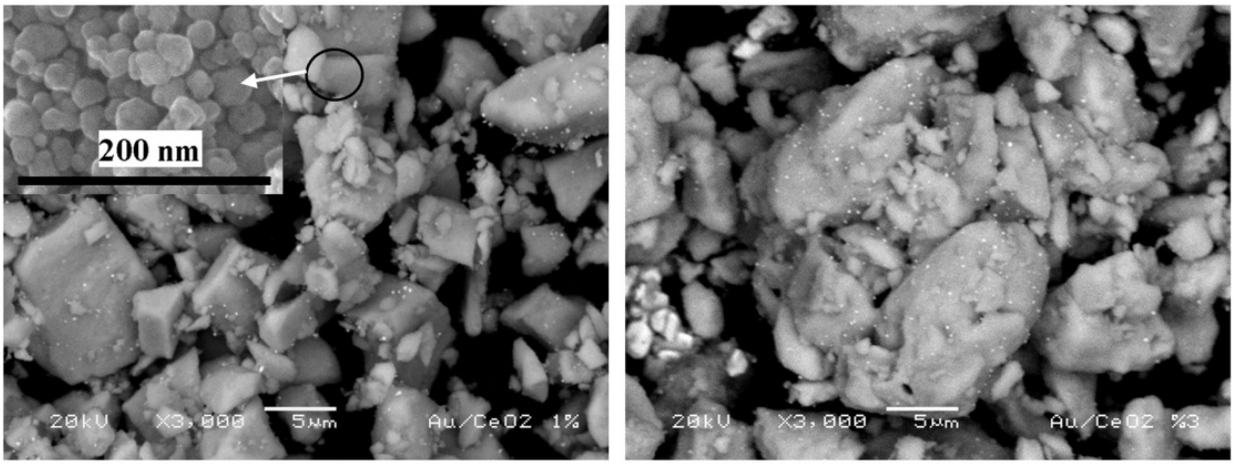

Figure 6. SEM image of: (a) 1Au/CeO_2 catalyst. Inset image corresponds to CeO_2 support obtained by FE-SEM. (b) 3Au/CeO_2 catalyst.

Figure 7 showed the XRD patterns of the 1Au/CeO_2 and 3Au/CeO_2 catalysts. It is possible to observe on the XRD pattern; characteristic peaks of the metallic gold and the others corresponding to the fluorite structure of ceria (CeO_2-cerianite). In addition, it is clear that the intensity of the diffraction peaks of the Au^0 increases proportionally as the Au was loading on CeO_2 suggesting on this sample a big Au crystallite size. The diffraction patterns of the Au/CeO_2 samples showed considerable line widths and no overlapping Au and CeO_2 diffraction peaks. We use the peaks display in the 35-45 = 2θ range to estimate the average Au crystallite size. The average value of the CeO_2 and the Au metal crystallite sizes on 1Au/CeO_2 and 3Au/CeO_2 samples were determined by Scherrer equation and it corresponds to 19, 23 and 33 nm respectively.

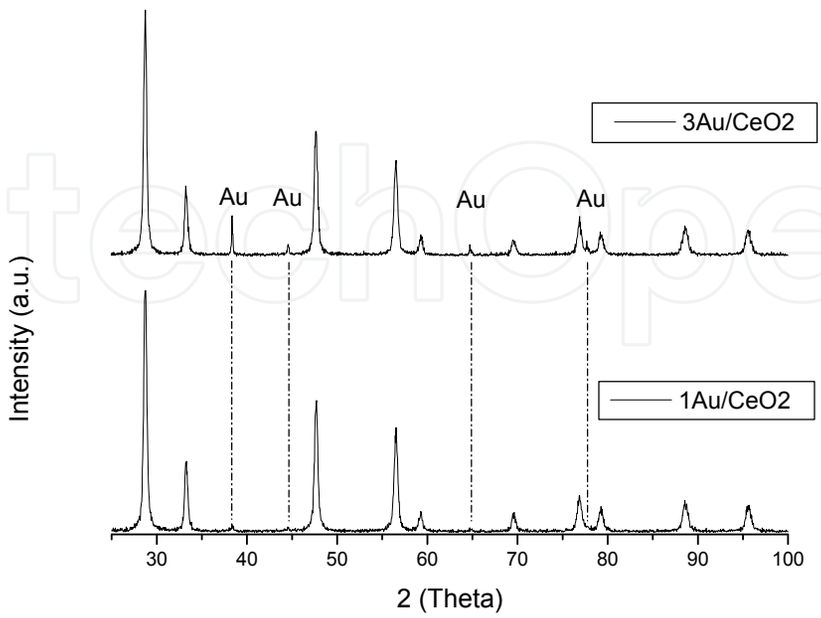

Figure 7. X ray diffraction patterns of the 1Au/CeO_2 and 3Au/CeO_2 catalysts. Cubic structure CeO_2 (fluorite structure) and characteristic peaks of the metallic gold.

TEM analysis of the 1Au/CeO_2 catalyst is showed on Figure 8a; it is possible to observe the homogeneous distribution of the CeO_2 particles about 20 nm of diameter. This value is close to the FE-SEM observation and the results calculated by Scherrer equation. High resolution image of Au nanoparticle (Figure 8b) revealed that after thermal treatments, the Au nanoparticle generally had a hemi-spherical shape. The Au particle size measure was ~ 17 nm. Analysis of the electron diffraction patterns of the Au nanostructures, inset on Figure 8b, show that the crystalline structure grows as a gold fcc single crystal. These Au nanoparticles was recorded along [110] orientation. Figure 8c showed the TEM image of the 3Au/CeO_2 catalyst, inset image on Figure 8c, showed the EDS spectra of the CeO_2 support and a gold nanoparticle the last one about 30 nm of diameter.

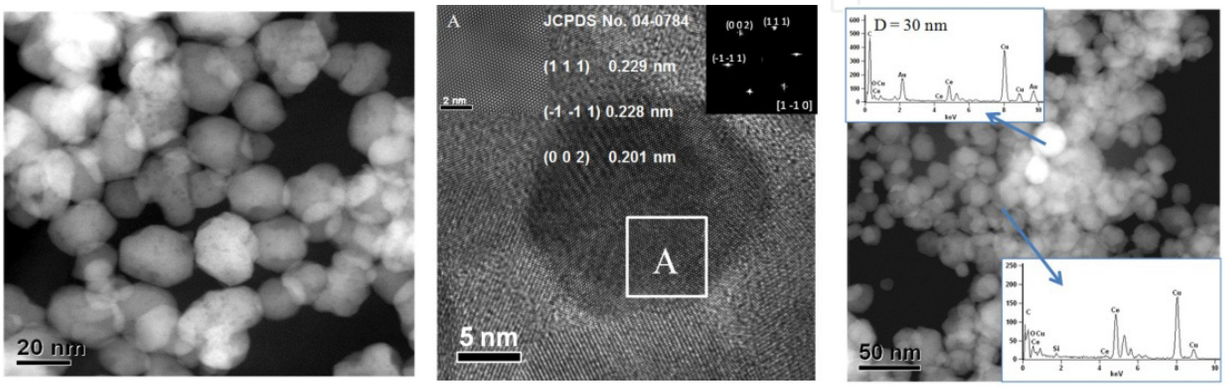

Figure 8. a) Low magnification TEM images of the 1Au/CeO_2 catalyst. b) HRTEM image of the Au nanoparticle from 1Au/CeO_2 catalyst which was recorded along [110] orientation. The d-spacing measured is showed inset image. The particle size was about 17 nm. c) Low magnification TEM images of the 3Au/CeO_2 image. Inset images showed the EDS spectra of the Au nanoparticle about 30 nm of diameter and CeO_2 support.

The TPR profiles of the Au-base catalysts deposited on CeO_2 are depicted in Figure 9. This technique was also employed to found the optimal reduction temperature in the catalysts. TPR profiles showed differences in the hydrogen consumption depending of the gold content. Reduction of Au/CeO_2 samples were observed from 150 to 330 °C. For this reason, the catalysts were first activated in H_2 stream at 350 °C before all the characterization. As reported in literature, pure CeO_2 showed two reduction peaks at about 500 and 800 ° C, and were interpreted as the reduction of surface capping oxygen and bulk phase lattice oxygen, respectively [26; 73]. For Au/CeO_2 catalysts, the peak assigned to ceria surface layer reduction was reported from 120 to 178 °C [54; 74]. In our calcined 1Au/CeO_2 catalyst, the hydrogen consumption peaks were observed within temperature range 175-325 °C, which could be deconvoluted into three components at reduction temperatures of 215, 257 and 294 °C respectively. Whereas, the calcined 3Au/CeO_2 catalyst exhibited a broad reduction peak, which could be decompounds into three components at reduction temperatures of 184, 267 and 297 °C. It is clear that the intensity of the peak at 257 °C observed on the 1Au/CeO_2 sample diminish significantly, and was shifted to the high-temperature region when the amount of Au was increased, because, the large crystallites tend to be reduced slower than

the small ones due to their relatively lower surface area exposed to H_2. Rodriguez et al. Showed by XAFS that Au facilitates the oxide reduction of the matrix respect to pure ceria [75]. Andreeva et al. [52] observed by TPR technique two reducible species on Au-CeO_2 samples. The low-temperature peak on the TPR profile was connected with the reduction of the oxygen species on the fine gold particles, and the high-temperature peak was due to the reduction of the surface ceria. Taking into account these results and the differences in the gold loading in our samples, we assume that the former peak corresponds to the reduction of Au oxide nanoparticles, then it causes spill-over of hydrogen onto the support inducing a concurrent reduction of both the Au oxide and the surface of CeO_2 as was reported on other Ce-base catalysts [26; 28; 52].

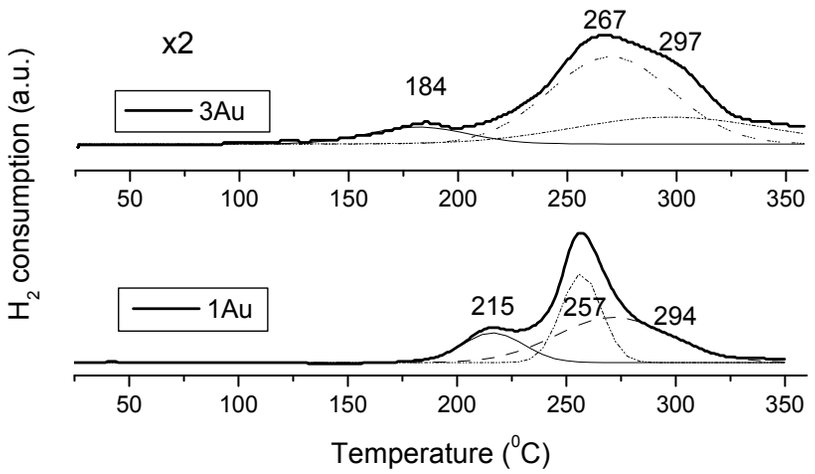

Figure 9. TPR profiles of the fresh Au/CeO_2 catalysts calcined at 400 °C.

The catalytic activity of the Au/CeO_2 catalysts as a function of the reaction temperature on the steam reforming of methanol reaction is presented on Figure 10. The light-off temperature of both samples started at ~ 350 °C at the molar CH_3OH/H_2O = 2.4 ratio, and the activity increased as temperature was rising. At the maximum reaction temperature, the methanol conversion observed on the 1Au/CeO_2 and 3Au/CeO_2 catalysts was 95 and 90 % respectively. The better catalytic activity observed on the 1Au/CeO_2 sample than on the 3Au/CeO_2 catalyst, could be attributed to differences in the Au particle size how was observed by XRD, SEM and TEM analysis. So, on the 3Au/CeO_2 catalyst the Au particle size was bigger than on the 1Au/CeO_2 catalyst. Croy et al. [76] studied the H_2 production through methanol decomposition on Pt/TiO_2 catalysts. They observed high catalytic activity on the catalysts with small particle size and diminish as the particle size increase. On methane combustion was observed better catalytic activity on the catalyst with low gold loading than the one with high gold loading, this result was associated with the dispersion of Au and the atomic ratio of Au^{3+}/Au^0 [77; 78]. However, Guzman and Gates [79] not found evidence between the Au cluster size and the catalytic activity on Au/MgO catalyst during the CO oxidation reaction with EXAFS technique. Wang et al. [80] suggested that the active sites in Au-ceria catalysts for the WGS probably contain Au nanoparticles and partially reduced ceria. It has been suggested that the presence of gold clusters weakens the bonding of the oxygen species on CeO_2 and facilitates the formation of more reactive species [53; 80; 81].

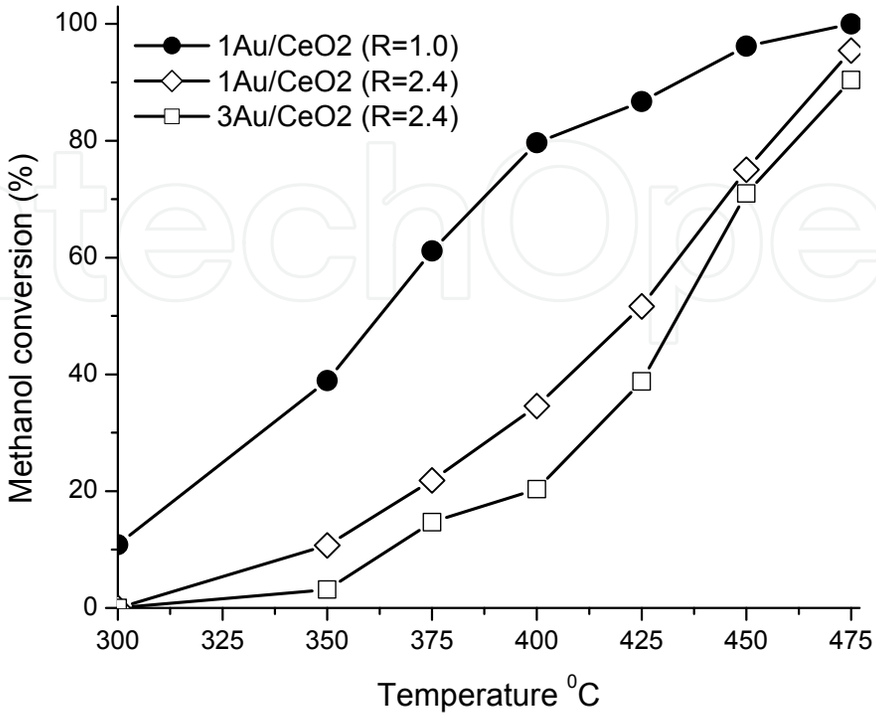

Figure 10. Temperature dependence of SRM activity of Au/CeO_2 catalysts. Partial pressure of CH_3OH and H_2O was 9999.18 and 1699.86 Pa respectively. GHVS=30,000 h^{-1}. The molar ratio in the steam was CH_3OH (1.95μmol)/H_2O (1.97 μmol) = R ≈ 1.0 and CH_3OH (4.7 μmol)/H_2O (1.97 μmol) = R ≈ 2.4.

The effect of the molar CH_3OH/H_2O ratio was evaluated on the $1Au/CeO_2$ catalyst and presented on Figure 10. It showed clearly that this sample had better catalytic activity when the molar CH_3OH/H_2O ratio is close to R = 1 than on the R = 2.4. At the beginning of the reaction (300 °C) the conversion of methanol was 11 % and, increase when the temperature was rising. At 375 °C the catalyst reached near 61 % conversion whereas on the R = 2.4 ratio the methanol conversion only reached ~ 22 %. This effect is caused by the modification on the feed concentrations of the fuel as was reported on [82]. The methanol conversion observed at the maximum reaction temperature, reached almost 100 % on the molar CH_3OH/H_2O ratio R = 1, while on the R = 2.4 ratio only 95 % conversion was observed. This finding suggests that the methanol is adsorbed preferable on the surface of the catalysts than water. Table 2 showed the catalytic performance on steam reforming of methanol reaction from 300 to 475 °C range of the bare CeO_2 and $1Au/CeO_2$ catalyst using the molar CH_3OH/H_2O ratio R = 1. As it can be seen, CeO_2 support showed low catalytic activity in almost all temperature range. However, at the end of the reaction the methanol conversion is almost 100 % for these samples. This finding showed the effect of the gold nanoparticles on CeO_2 during the catalytic activity. Gazsi et al. [83] suggested a cooperative effect between Au nanoparticles and CeO_2 support on the decomposition and reforming of methanol as was reported for other catalysts [9; 26; 64; 84].

Temperature (°C)	CeO_2 Methanol conversion and selectivity (%)					$1Au/CeO_2$ Methanol conversion and selectivity (%)				
	Conv.	H_2	CH_4	CO	CO_2	Conv.	H_2	CH_4	CO	CO_2
300	9.2	0	0	41.5	58.5	10.8	51.6	0	O	48.4
350	8.7	0	0	71.4	28.6	39.0	52.4	0.8	0.1	46.7
400	18.2	74.8	7.4	14.2	3.5	79.7	81.5	1.7	3.0	13.8
425	43.5	60.7	13.1	21.8	4.4	86.7	86.5	2.3	7.1	4.1
450	83.6	54.7	13.0	27.4	4.9	96.2	84.4	3.0	10.5	2.1
475	100	58.2	7.5	28.6	5.7	100	84.4	3.1	10.6	1.9

Table 2. Catalytic activity of the bare CeO_2 and $1Au/CeO_2$ catalyst. The molar ratio in the steam was CH_3OH (1.95μmol)/H_2O (1.97 μmol) = R ≈ 1.0

The reaction products observed on the steam reforming of methanol reaction of the Au/CeO_2 catalysts were H_2, CO, CO_2, CH_4 and H_2O. Small production of methyl formate as by-product of the reaction was observed in both samples. Figure 11a showed the distribution of hydrogen on the Au-base catalysts. Higher H_2 production was observed from 300 to 400 °C range on the catalysts tested with high molar CH_3OH/H_2O ratio R = 2.4 than R = 1. The drop of the hydrogen selectivity at higher temperatures could be attributed at the formation of CH_4. At the beginning of the reaction all samples showed low CO selectivity, Figure 11b. However, as the reaction temperature raise from 375 to 470 °C, the CO production increase and the selectivity toward CO_2 decrease. It is clear from Figure 11b that the $3Au/CeO_2$ sample showed high selectivity toward CO than on the $1AuCeO_2$ sample. In addition, we observed that the CO production is practically the same on the $1AuCeO_2$ catalyst (~ 10 %) independently of the molar CH_3OH/H_2O ratio. Table 2 showed the selectivity of the bare CeO_2 compared with $1Au/CeO_2$ catalyst. It showed the beneficial effect of the gold nanoparticles on the CeO_2. Because, the selectivity toward undesirable by-products such as CO and CH_4 observed on the bare CeO_2, were drop on the $1Au/CeO_2$ catalyst and the selectivity toward H_2 was improved on this catalyst.

Time on-stream studies (Fig. 12) at 350 °C in the $1Au/CeO_2$ sample with CH_3OH/H_2O ratio = 1.0, reveal high stability on the activity during the steam reforming of methanol reaction during a 65 h of reaction period, as well as high stability in the reaction products. The stability of catalysts under operating conditions is desirable for commercial applications. Fu et al. [73] found no significant change in activity after 120 h on stream on WGS. This behavior could be suggested that the catalyst maintains the same catalytic species during the SRM reaction and it does not lose by effect of the reaction conditions. So, these results showed that the CeO_2 matrix could be use to prevent the vanished of active phase during the reaction. Thus, a cooperative redox mechanism for the SRM reaction on Au–ceria is possible, similar to Cu–ceria or another kind of catalysts [26; 37; 63; 64; 73; 85] and for the WGS reaction [73].

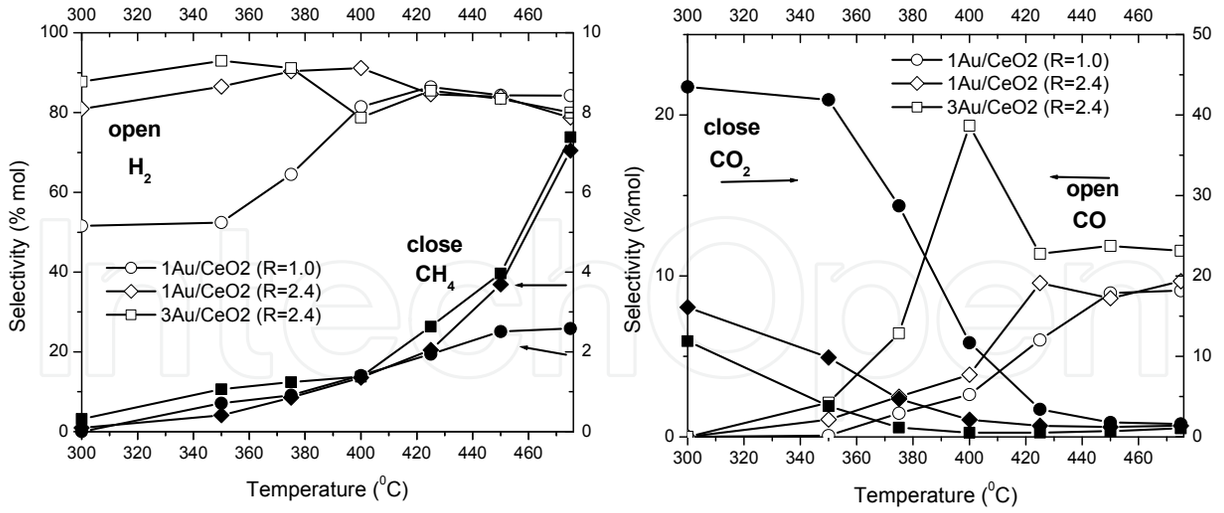

Figure 11. a) H_2 and CH_4 selectivity as a function of reaction temperature. b) CO and CO_2 selectivity as a function of reaction temperature. Partial pressure of CH_3OH and H_2O was 9999.18 and 1699.86 Pa respectively. GHVS=30,000 h^{-1}. The molar ratio in the steam was CH_3OH (1.95μmol)/H_2O (1.97 μmol) = R ≈ 1.0 and CH_3OH (4.7 μmol)/H2O (1.97 μmol) = R ≈ 2.4.

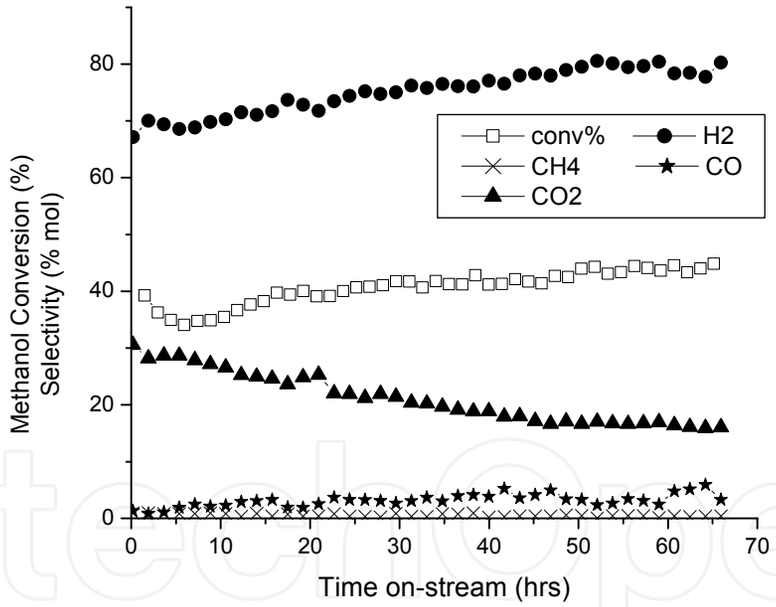

Figure 12. Stability of 1Au/CeO_2 catalyst at 350 °C. Partial pressure of CH_3OH and H_2O was 9999.18 and 1699.86 Pa respectively. GHVS=30,000 h^{-1}. The molar ratio in the steam was CH_3OH (1.95μmol)/H_2O (1.97 μmol) = R ≈ 1.0

5. Conclusion

Cu/CeO_2, Ni/CeO_2 and three bimetallic copper-nickel catalysts supported on CeO_2 were prepared by the impregnation method and tested in the OSRM reaction. The monometallic Ni/CeO_2 and the bimetallic Cu-Ni/CeO_2 (synthesized by co-impregnation) catalysts demonstrate both a higher catalytic activity in the OSRM reaction than the other catalysts. CO-

chemisorption followed by DRIFT technique showed differences in the former samples. So, in the Ni/CeO_2 and $Cu\text{-}Ni/CeO_2$ catalysts was observed a band at 1625 cm^{-1} that was not present on the bimetallic samples prepared by successive impregnation as well for the Cu/CeO_2 samples which indicates that CO does not adsorb on these materials. This suggests that the metal active phase blockage some sites on the support or the active phase, modifies the surface of the catalyst for the adsorption of methanol and water inhibited the catalytic reaction on this system. In the case of the Au/CeO_2 system, nanosized ceria was prepared in advance with particle size of 19 nm and used as a support for gold nanoparticles. The average Au crystallite size in the $1Au/CeO_2$ and $3Au/CeO_2$ catalysts was 21 and 31 nm respectively. Differences in the reducibility of the Au/CeO_2 catalysts were observed depending of the Au loading. H_2-TPR results showed a shift of the reduction peaks toward high-temperature when the amount of Au was increased associated with the Au particle size present on the catalysts. The gold-base catalysts supported on CeO_2 showed catalytic activity on the SRM reaction and high selectivity toward H_2. Among these catalysts the sample with small Au particle size showed best performance in methanol conversion than on the catalyst with big Au particle size. These finding show the relationship between the Au particle size and the catalytic activity. In addition, it was demonstrate the beneficial effect of gold nanoparticles on the catalytic activity, as well as on the selectivity toward undesirable by-products such as CO and CH_4 and the selectivity toward H_2. The stability of the $1Au/CeO_2$ catalyst at 350 °C was followed as a function of time on stream. This result showed high stability during the reaction. It is assumed that the interface between Au and partially reduced ceria is responsible for the high activity of Au/CeO_2 catalyst. In general we observed different behavior in the catalytic activity in our catalysts in the OSRM reaction to those reported in the literature. This difference could be attributed to the nature of the metal active phase and metal addition to the support. In this way, we suggest that the OSRM reaction could be a structure sensitive reaction according with the literature. However, further work is needed to refine and optimize the catalysts to improve the methanol conversion to produce CO-free hydrogen from the reaction under study.

Author details

Raúl Pérez-Hernández*, Demetrio Mendoza-Anaya and Albina Gutiérrez Martínez
Instituto Nacional de Investigaciones Nucleares, Carr. México-Toluca S/N La Marquesa, Ocoyoacac, México

Antonio Gómez-Cortés
Instituto de Física-Universidad Nacional Autónoma de México, D.F., México

Acknowledgement

Thanks to C. Salinas for technical support and to the projects ININ-CA-009 and CONACYT CB-2008-01-104540 for financial support. Authors would like to acknowledge Dr. Carlos Ángeles for its valuable comments and suggestions on the manuscript.

* Corresponding Author

6. References

[1] Armor, J. N. (1999) The multiple roles for catalysis in the production of H_2. Appl. Catal. A: Gen. 159-176: 159.

[2] Peña, M. A., J. P. Gómez, and J. L. G. Fierro (1996) New catalytic routes for syngas and hydrogen production. Appl. Catal. A: Gen. 144: 7-57.

[3] Pakulska, M. M., C. M. Grgicak, and J. B. Giorgi (2007) The effect of metal and support particle size on NiO/CeO_2 and NiO/ZrO_2 catalyst activity in complete methane oxidation. Appl Catal A: Gen. 332: 124-129.

[4] Sprung, C., B. Arstad, and U. Olsbye (2011) Methane Steam Reforming Over $Ni/NiAl_2O_4$ Catalyst: The Effect of Steam-to-Methane Ratio. Top Catal 54: 1063-1069.

[5] Montoya, J. A., E. Romero-Pascual, C. Gimon, P. D. Angel, and A. Monzón (2000) Methane reforming with CO_2 over Ni/ZrO_2-CeO_2 catalysts prepared by sol-gel. Catal Today. 63: 71-85.

[6] Roh, H.-S., K.-W. Jun, W.-S. Dong, J.-S. Chang, S.-E. Park, and Y.-I. Joe (2002) Highly active and stable Ni/Ce-ZrO2 catalyst for H2 production from methane. J. Mol Catal A: Chemical. 181: 137-142.

[7] Takeguchi, T., S.-n. Furukawa, and M. Inoue (2001) Hydrogen Spillover from NiO to the Large Surface Area CeO_2-ZrO_2 Solid Solutions and Activity of the NiO/CeO_2-ZrO_2 Catalysts for Partial Oxidation of Methane. J. Catal. 202: 14-24.

[8] Matsumura, Y., and T. Nakamori (2004) Steam Reforming of Methane over Nickel Catalysts. Appl. Catal. A: Gen. 258: 107-114.

[9] Agrell, J., H. Birgersson, M. Boutonnet, I. Melián-Cabreara, R. M. Navarro, and J. L. G. Fierro (2003) Production of hydrogen from methanol over Cu/ZnO catalysts promoted by ZrO_2 and Al_2O_3. J Catal 219: 389-403.

[10] Lindström, B., and L. J. Pettersson (2001) Hydrogen generation by steam reforming of methanol over copper-based catalysts for fuel cell applications. Int J Hydrogen Energy. 26: 923-933.

[11] Agrell, J., M. Boutonnet, and J. L. G. Fierro (2003) Production of hydrogen from methanol over binary Cu/ZnO catalysts: Part II. Catalytic activity and reaction pathways. Appl. Catal. A: Gen. 253: 213-223.

[12] Purnama, H., F. Girgsdies, T. Ressler, J. H. Schattka, R. A. Caruso, R. Scomäcker, and R. Schlögl (2004) CO formation/selectivity for steam reforming of methanol with a commercial $CuO/ZnO/Al_2O_3$ catalyst Catal Lett. . 94 61-68.

[13] Breen, J. P., and J. R. H. Ross (1999) Methanol reforming for fuel-cell applications: development of zirconia-containing Cu–Zn–Al catalysts. Catal. Today. 51 521-533.

[14] Günter, M. M., T. Ressler, R. E. Jentoft, and B. Bems (2001) Redox Behavior of Copper Oxide/Zinc Oxide Catalysts in the Steam Reforming of Methanol Studied by in Situ X-Ray Diffraction and Absorption Spectroscopy J. Catal. 203: 133-149.

[15] Fukahori, S., H. Koga, T. Kitaoka, A. Tomoda, R. Suzuki, and H. Wariishi (2006) Hydrogen production from methanol using a SiC fiber-containing paper composite impregnated with Cu/ZnO catalyst Appl. Catal. A: Gen. . 310 138-144.

[16] Fierro, G., M. L. Jacono, M. Inversi, P. Porta, F. Cioci, and R. Lavecchia (1996) Study of the reducibility of copper in CuO-ZnO catalysts by temperature-programmed reduction. Appl. Catal. A: Gen. . 137 327-348.

[17] Fujitani, T., and J. Nakamura (2000) The chemical modification seen in the Cu/ZnO methanol synthesis catalysts Appl. Catal. A: Gen. 191 111-129.

[18] Bowker, M., R. A. Hadden, H. Houghton, J. N. K. Hyland, and K. C. Waugh (1988) The mechanism of methanol synthesis on copper/zinc oxide/alumina catalysts J. Catal. . 109 263-273.

[19] Duprez, D., Z. Ferhat-Hamida, and M. M. Bettahar (1990) Surface mobility and reactivity of oxygen species on a copper-zinc catalyst in methanol synthesis J. Catal. . 124: 1-11.

[20] Yong-Feng, L., D. Xin-Fa, and L. Wei-Ming (2004) Effects of ZrO2-promoter on catalytic performance of CuZnAlO catalysts for production of hydrogen by steam reforming of methanol Int. J. Hydrogen Energy. 29: 1617- 1621.

[21] Szizybalski, A., F. Girgsdies, A. Rabis, Y. Wang, M. Niederberger, and T. Ressler (2005) In situ investigations of structure-activity relationships of a Cu/ZrO_2 catalyst for the steam reforming of methanol. J Catal. . 233: 297-307.

[22] Oguchi, H., T. Nishiguchia, T. Matsumotoa, H. Kanaia, K. Utania, Y. Matsumurab, and S. Imamura (2005) Steam reforming of methanol over $Cu/CeO_2/ZrO_2$ catalysts. Appl Catal A: Gen. 281: 69-73.

[23] Oguchi, H., H. Kanai, K. Utani, Y. Matsumura, and S. Imamura (2005) Cu_2O as active species in the steam reforming of methanol by CuO/ZrO_2 catalysts Appl. Catal. A 293 64-70.

[24] Cheng, W.-H., I. Chen, J.-S. Liou, and S.-S. Lin (2003) Supported Cu Catalysts with Yttria-Doped Ceria for Steam Reforming of Methanol Topics Catal. 22 225-233.

[25] Liu, Y., T. Hayakawa, K. Suzuki, and S. Hamakawa (2001) Production of hydrogen by steam reforming of methanol over Cu/CeO_2 catalysts derived from $Ce_{1-x}Cu_xO_{2-x}$ precursors Catal. Commun. . 2: 195-200.

[26] Pérez-Hernández, R., A. Gutiérrez-Martínez, and C. E. Gutiérrez-Wing (2007) Effect of Cu loading on CeO_2 for hydrogen production by oxidative steam reforming of methanol. Int J Hydrogen Energy. 32: 2888-2894.

[27] Zhang, X., and P. Shi (2003) Production of hydrogen by steam reforming of methanol on CeO_2 promoted Cu/Al_2O_3 catalysts J. Mol. Catal. A: Chem. 194: 99-105.

[28] Pérez-Hernández, R., F. Aguilar, A.Gomés-Cortés, and G. Díaz (2005) NO reduction with CH_4 or CO on Pt/ZrO_2-CeO_2 catalysts. Catal. Today. 107-108: 175-180.

[29] Trovarelli, A., C. De-Leitenburg, M. Boaro, and G. Dolcetti (1999) The utilization of ceria in industrial catalysis. Catal. Today. 50: 353-367.

[30] Mastalir, A., B. Frank, A. Szizybalski, H. Soerijanto, A. Deshpande, M. Niederberger, R. Schomacker, R. Schlogl, and T. Ressler (2005) Steam reforming of methanol over $Cu/ZrO_2/CeO_2$ catalysts: a kinetic study J. Catal. 230 464-475.

[31] Ritzkopf, I., S. Vukojevic´, C. Weidenthaler, J. D. Grunwaldt, and F. Smith (2006) Decreased CO production in methanol steam reforming over Cu/ZrO_2 catalysts prepared by the microemulsion technique Appl. Catal. Gen. A. 302 215-223.

[32] Breen, J. P., F. C. Meunier, and J. R. H. Ross (1999) Mechanistic aspects of the steam reforming of methanol over a $CuO/ZnO/ZrO_2/Al_2O_3$ catalyst. Chem. Commun.: 2247-2248.

[33] Wang, L.-C., Q. Liu, M. Chen, Y.-M. Liu, Y. Cao, H.-Y. He, and K.-N. Fan (2007) Structural Evolution and Catalytic Properties of Nanostructured Cu/ZrO_2 Catalysts Prepared by Oxalate Gel-Coprecipitation Technique. J. Phys. Chem. C. 111 16549-16557.

[34] Yao, C.-Z., L.-C. Wang, Y.-M. Liu, G.-S. Wu, Y. Cao, W.-L. Dai, H.-Y. He, and K.-N. Fan (2006) Effect of preparation method on the hydrogen production from methanol steam reforming over binary Cu/ZrO_2 catalysts. Appl Catal A: Gen 297: 151-158.

[35] Lindström, B., L. J. Pettersson, and P. G. Menon (2002) Activity and characterization of Cu/Zn, Cu/Cr and Cu/Zr on g-alumina for methanol reforming for fuel cell vehicles Appl. Catal. Gen. A. 234 111-125.

[36] Jeong, H., K. Kim, T. Kim, C. Ko, H. Park, and I. Song (2006) Hydrogen production by steam reforming of methanol in a micro-channel reactor coated with $Cu/ZnO/ZrO_2/Al_2O_3$ catalyst. J. Power Sources. 159 1296-1299.

[37] Pérez-Hernández, R., G. Mondragón-Galicia, D. Mendoza-Anaya, J. Palacios, C. Angeles-Chavez, and J. Arenas-Alatorre (2008) Synthesis and characterization of bimetallic $Cu–Ni/ZrO_2$ nanocatalysts: H_2 production by oxidative steam reforming of methanol. Int J Hydrogen Energy. 33: 4569-4576.

[38] Pérez-Hernández, R., A. Gutiérrez-Martínez, J. Palacios, M. Vega-Hernández, and V. Rodríguez-Lugo (2011) Hydrogen production by oxidative steam reforming of methanol over Ni/CeO_2-ZrO_2 catalysts. Int J Hydrogen Energy. 36: 6601- 6608.

[39] López, P., G. Mondragón-Galicia, M. E. Espinosa-Pesqueira, D. Mendoza-Anaya, M. E. Fernández, A. Gómez-Cortés, J. Bonifacio, G. Martínez-Barrera, and R. Pérez-Hernández (2012) Hydrogen production from Oxidative Steam Reforming of Methanol: Effect of the Cu and Ni Impregnation on ZrO_2 and their molecular simulation studies. Int J Hydrogen Energy. 37: 9018-9027.

[40] Yang, Y., J. Ma, and E. Wu (2006) Production of hydrogen by steam reforming of ethanol over a Ni/ZnO catalyst. Int J Hydrogen Energy. 31 877-882.

[41] Biswas, P., and D. Kunzru (2007) Steam reforming of ethanol for production of hydrogen over $Ni/CeO_2–ZrO_2$ catalyst: Effect of support and metal loading Int J Hydrogen Energy 32 969-980.

[42] Mariño, F. J., E. G. Cerrella, S. Duhalde, M. Jobbagy, and M. Lombarde (1998) Hydrogen from steam reforming of ethanol. Characterization and performance of copper–nickel supported catalysts. Int J Hydrogen Energy 23 1095-1101.

[43] Mariño, F. J., M. Boveri, G. Baronetti, and M. Lombarde (2001) Hydrogen production from steam reforming of bioethanol using Cu/Ni/K/γ-Al_2O_3 catalysts. Effect of Ni. Int J Hydrogen Energy 26 665-668.

[44] Sun, J., X.-P. Qui, F. Wu, and W.-T. Zhu (2005) H_2 from steam reforming of ethanol at low temperaure over Ni/Y_2O_3, Ni/La_2O_3 and Ni/Al_2O_3 catalysts for fuel cell application. Int. J. Hydrogen energy. 30: 437-445.

[45] Navarro, R. M., M. C. Álvarez-Galván, F. Rosa, and J. L. G. Fierro (2006) Hydrogen production by oxidative steam reforming of hexadecane over Ni and Pt catalysts supported on Ce/La-doped Al_2O_3 Appl. Catal. A: Gen. 297: 60-72.

[46] Xia, B. J., J. D. Holladay, R. A. Dagle, E. O. Jones, and Y. Wang (2005) Development of highly active Pd-ZnO/Al_2O_3 catalysts for microscale fuel processor applications. Chem Eng Technol. 28(4): 515-519.

[47] Iwasa, N., S. Masuda, N. Ogawa, and N. Takezawa (1995) Steam reforming of methanol over Pd/ZnO: Effect of the formation of PdZn alloys upon the reaction. Appl Catal A: Gen. 125(1): 145-157.

[48] Karim, A. M., T. Conant, and A. Datye (2006) The role of PdZn alloy formation and particle size on the selectivity for steam reforming of methanol. J Catal 243(2): 420-427.

[49] Pérez-Hernández, R., A. D. Avendaño, E. Rosas, and V. Rodríguez (2011) Hydrogen Production by Methanol steam reforming over Pd/ZrO_2-TiO_2 catalysts. Topic Catal. . 54: 572-578.

[50] Haruta, M., T. Tsubota, T. Kobayashi, H. Kageyama, M. J. Genet, and B. Delmon (1993) Low-Temperature Oxidation of CO over Gold Supported on TiO_2, a-Fe_2O_3, and Co_3O_4. J. Catal. 144: 175.

[51] Trovarelli, C. A. (1996) Catalytic properties of ceria and CeO_2-containing materials. Catal. Rev. Sci. Eng. . 38: 439.

[52] Andreeva, D., V. Idakiev, T. Tabakova, L. Ilieva, P. Falaras, A. Bourlinos, and A. Travlos (2005) Low-temperature water-gas shift reaction over Au/CeO_2 catalysts. Catal. Today. 72: 51-57.

[53] Fu, Q., H.Saltsburg, and M. Flytzani-Stephanopoulos (2003) Active non-metallic Au and Pt species on Ceria-based Water-gas shift Catalysts. Science 301: 935-938.

[54] Sandoval, A., A. Gómez-Cortés, R. Zanella, G. Díaz, and J. M. Saniger (2007) Gold nanoparticles: Support effects for the WGS reaction. J. Mol Catal A: Chemical. 278: 200.

[55] Scire, S., S. Minnico, C. Crisafulli, C. Satriano, and A. Pistone (2003) Catalytic combustion of volatile organic compounds on gold/cerium oxide catalysts. Appl. Catal. B: Environmental. 40: 43.

[56] Panzera, G., V. Modafferi, S. Candamano, A. Donato, F. Frusteri, and P. L. Antonucci (2004) CO selective oxidation on ceria-supported Au catalysts for fuel cell application. J . Power Sources 135: 177.

[57] Manzoli, M., F. Boccuzzi, A. Chiorino, F. Vindigni, W. Deng, and M. Flytzani-Stephanopoulos (2007) Spectroscopic features and reactivity of CO adsorbed on different Au/CeO_2 catalysts. J Catal 245: 308.

[58] Chang, F.-W., H.-Y. Yu, L. S. Roselin, and H.-C. Yang (2005) Production of hydrogen via partial oxidation of methanol over Au/TiO_2 catalysts. Appl. Catal. A: General 290: 138.

[59] Pérez-Hernández, R., A. Gutiérrez-Martínez, A. Mayoral, F. L. Deepak, M. E. Fernández-García, G. Mondragón-Galicia, M. Miki, and M. Jose-Yacaman (2010) Hydrogen Production by Steam Reforming of Methanol over a Ag/ZnO One Dimensional Catalyst. Advanced Materials Research. 132: 205-219.

[60] Pérez-Hernández, R., and C. Gutiérrez-Wing (2009) Design of new Ag-Au(1-D)-CeO_2 catalysts for hydrogen production by steam reforming of methanol. EuropaCat IX, Salamanca, Spain. 1-3.

[61] Pérez-Hernández, R., A. Gutiérrez-Martínez, and C. Gutiérrez-Wing (2010) Hydrogen Production by Steam Reforming of Methanol over New Ag-Au(1-D)-CeO_2 Catalyst. Mater. Res. Soc. Symp. Proc. Vol. 127, Materials Research Society. 127: 1-4.

[62] Pérez-Hernández, R., A. Gómez-Cortés, J. Arenas-Alatorre, S. Rojas, R. Mariscal, J. L. G. Fierro, and G. Díaz (2005) SCR of NO by CH_4 on Pt/ZrO_2-TiO_2 sol-gel catalysts. Catal. Today. 107-108: 149-156.

[63] Pérez-Hernández, R., L. C. Longoria, J. Palacios, M. M. Aguila, and V. Rodríguez (2008) Oxidative steam reforming of methanol for hydrogen production over Cu/CeO_2-ZrO_2 catalysts. Energ Mater Mater Sci Eng Energ Syst. 3: 152-157.

[64] Pérez-Hernández, R., D. Mendoza-Anaya, M. E. Fernández, and A. Gómez-Cortés (2008) Synthesis of mixed ZrO_2-TiO_2 oxides by sol-gel: Microstructural characterization and infrared spectroscopy studies of NOx. J. Mol Catal A: Chemical 281: 200-206.

[65] Arenas-Alatorre, J., A. Gómez-Cortés, M. Avalos-Borja, and G. Díaz (2005) Surface Properties of Ni-Pt/SiO_2 Catalysts for N_2O Decomposition and Reduction by H_2. . J Phys Chem B. 109: 2371.

[66] Ratnasamy, P., D. Srinivas, C. V. V. Satyanarayana, P. Manikandan, R. Senthil-Kumaran, M. Sachin, and V. N. Shetti (2004) Influence of the support on the preferential oxidation of CO in hydrogen-rich steam reformates over the CuO-CeO_2-ZrO_2 system. . J Catal. 221: 455-465.

[67] Harrison, P. G., I. K. Ball, W. Azelee, W. Daniell, and F. Goldfarb (2000) Nature and surface redox properties of copper(ii)-promoted cerium(IV) oxide COoxidation catalysts. Chem Mater. 12: 3715-3725.

[68] Turco, M., G. Bagnasco, U. Costantino, F. Marmottini, T. Montanari, G. Ramis, and G. Busca (2004) Production of hydrogen from oxidative steam reforming of methanol II.

Catalytic activity and reaction mechanism on Cu/ZnO/Al_2O_3 hydrotalcite-derived catalysts. J. Catal. 228: 56.

[69] Hollins, P. (1992) Surf. Sci. Rep. . 16: 51.

[70] Sakakini, B. H., J. Tabatabaei, M. J. Watson, and K.C.Waugh (2000) J.Mol. Catal. A. 162 297.

[71] Nasser, H., Á. Rédey, T. Yuzhakova, and J. Kovács (2009) Thermal Stability and Surface Structure of Mo/CeO_2 and Ce-doped Mo/Al_2O_3 Catalysts. Journal of Thermal Analysis and Calorimetry. 95 69-74.

[72] Tabakova, T., F. Boccuzzi, M. Manzoli, and D. Andreva (2003) FTIR study of low-temperature water-gas shift reaction on gold/ceria catalyst. Appl Catal A: Gen. 252: 385-397.

[73] Fu, Q., W. Deng, H. Saltsburg, and M. Flytzani-Stephanopoulos (2005) Activity and stability of low-content gold–cerium oxide catalysts for the water–gas shift reaction Appl. Catal. B: Environmental. 56: 57-68.

[74] Ilieva, L., G. Pantaleo, I. Ivanov, A. M. Venezia, and D. Andreeva (2006) Gold catalysts supported on CeO_2 and CeO_2–Al_2O_3 for NOx reduction by CO Appl. Catal. B: Environmental. 65: 101-109.

[75] Rodriguez, J. A., X. Wang, P. Liu, W. Wen, J. C. Hanson, J. Hrbek, M. Pérez, and J. Evans (2007) Gold nanoparticles on ceria: importance of O vacancies in the activation of gold. Top. Catal. 44: 73-81.

[76] Croy, J. R., S. Mostafa, J. Liu, Y.-h. Sohn, and B. R. Cuenya (2007) Size dependent Study of MeOH decomposition over Size-selected Pt nanoparticles Synthesized via micelle Encapsulation. Catal. Lett. 118: 1.

[77] Zhang, Y., J. Deng, L. Zhang, W. Qiu, H. Dai, and H. He (2008) AuOx/$Ce_{0.6}Zr_{0.3}Y_{0.1}O_2$ nano-sized catalysts active for the oxidation of methane Catal. Today. 139: 29-36.

[78] Zhang, X., H. Shi, and B.Q. Xu (2007) Comparative study of Au/ZrO_2 catalysts in CO oxidation and 1,3-butadiene hydrogenation Catal. Today. 122: 330-337.

[79] Guzman, J., and B. C. Gates (2004) Catalysis by Supported Gold: Correlation between Catalytic Activity for CO Oxidation and Oxidation States of Gold J. Am. Chem. Soc. 126: 2672-2673.

[80] Wang, X., J. A. Rodriguez, J. C. Hanson, D. Gamarra, A.Martínez-Arias, and M. Fernández-García (2008) Ceria-based Catalysts for the Production of H2 Through the Water-gas-shift Reaction: Time-resolved XRD and XAFS Studies. Top. Catal. 49: 81-88.

[81] Guzman, J., S. Carrettin, J. C. Fierro-Gonzalez, Y. Hao, B. C. Gates, and A. Corma (2005) CO Oxidation Catalyzed by Supported Gold: Cooperation between Gold and Nanocrystalline Rare-Earth Supports Forms Reactive Surface Superoxide and Peroxide Species Angew. Chem. Int. Ed. 44: 4778-4781.

[82] Ahmed, S., and M. Krumpelt (2001) Hydrogen from hydrocarbon fuels for fuel cells. Int J Hydrogen Energy 26: 291.

[83] Gazsi, A., T. Bánsági, and F. Solymosi (2009) Hydrogen formation in the reaction of methanol on supported Au catalysts. Catal. Lett. 131: 33.
[84] Fisher, I. A., and A. T. Bell (1999) A Mechanistic Study of Methanol Decomposition over Cu/SiO_2, ZrO_2/SiO_2, and $Cu/ZrO_2/SiO_2$. J. Catal. . 184: 357.
[85] Burch, R. (2007) Gold catalysts for pure hydrogen production in the water–gas shift reaction: activity, structure and reaction mechanism Phys. Chem. Chem. Phys. 8: 5483-5500.